On the origin of cold dark matter halo density profiles

Yu Lu[1]⋆, H.J. Mo[1], Neal Katz[1], Martin D. Weinberg[1]

[1] *Department of Astronomy, University of Massachusetts, Amherst MA 01003-9305, USA*

ABSTRACT

N-body simulations predict that CDM halo-assembly occurs in two phases: 1) a fast accretion phase with a rapidly deepening potential well; and 2) a slow accretion phase characterised by a gentle addition of mass to the outer halo with little change in the inner potential well. We demonstrate, using one-dimensional simulations, that this two-phase accretion leads to CDM halos of the NFW form and provides physical insight into the properties of the mass accretion history that influence the final profile. Assuming that the velocities of CDM particles are effectively isotropised by fluctuations in the gravitational potential during the fast accretion phase, we show that gravitational collapse in this phase leads to an inner profile $\rho(r) \propto r^{-1}$. Slow accretion onto an established potential well leads to an outer profile with $\rho(r) \propto r^{-3}$. The concentration of a halo is determined by the fraction of mass that is accreted during the fast accretion phase. Using an ensemble of realistic mass accretion histories, we show that the model predictions of the dependence of halo concentration on halo formation time, and hence the dependence of halo concentration on halo mass, and the distribution of halo concentrations all match those found in cosmological *N*-body simulations. Using a simple analytic model that captures much of the important physics we show that the inner r^{-1} profile of CDM halos is a natural result of hierarchical mass assembly with a initial phase of rapid accretion.

Key words: dark matter - large-scale structure of the universe - galaxies: halos - methods: theoretical

1 INTRODUCTION

In the cold dark matter (CDM) paradigm of structure formation, most of the cosmic mass is locked in virialised clumps called dark matter halos. Luminous objects, galaxies and clusters of galaxies, are assumed to form in the potential wells of these dark matter halos. High resolution *N*-body simulations have shown that the density profiles of CDM halos can be fairly well described by a universal form,

$$\rho_{\rm NFW}(r) = \frac{4\rho_s}{(r/r_s)(1 + r/r_s)^2}, \qquad (1)$$

where r_s is a characteristic radius and ρ_s is a characteristic density (Navarro, Frenk & White 1996, 1997; hereafter (NFW). The value of r_s is often given in units of the virial radius and one over that value is referred to as the halo concentration. There is still uncertainty about the exact value of the inner slope. While some simulations indicate that the inner logarithmic slope may be steeper than the NFW value, −1 (e.g. Moore et al. 1999, Ghigna et al. 2000; Fukushige & Makino 1997, 2001, 2003), others give slopes shallower than −1 (Subramanian, Cen & Ostriker 2000; Taylor & Navarro 2001; Ricotti 2003). Jing & Suto (2000) found that CDM

halo profiles in their simulations do not have a completely universal form, with the inner slope changing from system to system.

Until now, there has not been a natural explanation for the approximate 'universal' profile resulting from the gravitational collapse of a CDM density field. The pioneering work by Gunn & Gott (1972) considered the collapse of uniform spherical perturbations of collisionless cold dark matter in an expanding background. This simple model explains some properties of virialised objects, such as their mean density and size, but does not describe the density profile of a collapsed object. Subsequently, the spherical collapse model was extended to incorporate realistic initial perturbations (e.g. Gott 1975; Gunn 1977; Fillmore & Goldreich 1984; Bertschinger 1985; Hoffman & Shaham 1985; Ryden & Gunn 1987; Ryden 1988; Zaroubi & Hoffman 1993). Bertschinger (1985) and Fillmore & Goldreich (1984) found that halos have similar asymptotic inner density profiles with $\rho(r) \propto r^{-\gamma}$ and $\gamma \sim 2$, for a wide range of initial density perturbations. Unfortunately, the inner slope predicted by such models is much steeper than that found in 3-dimensional cosmological simulations. A number of authors (e.g. White & Zaritsky 1992; Ryden 1993; Sikivie et al. 1997; Subramanian 2000; Subramanian et al. 2000; Hiotelis 2002; Le Delliou & Henriksen 2003; Shapiro et al. 2004; Barnes et

---

⋆ E-mail: luyu@astro.umass.edu

al. 2005) noticed that tangential motions of particles may cause flattening of the inner profiles. N-body simulations by Huss et al. (1999) and Hansen & Moore (2004) showed that the inner density profile of a halo is correlated with the degree of velocity anisotropy. However, none of these has provided clear dynamical mechanism for the origin of the 'univeral' $\rho(r) \propto r^{-1}$ inner profile observed in cosmological N-body simulations.

Lynden-Bell (1967) proposed that, as long as the initial condition for the collapse is clumpy, a final equilibrium state with a universal profile may be achieved as a result of violent relaxation that may cause a complete mixing of particles in phase space. Numerical simulations have shown that such collapses indeed produce a universal inner profile (van Albada 1982), but the relaxation is incomplete, in the sense that there is still a significant correlation between the final and initial states of a particle. Tremaine et al. (1986) provide statistical constraints on equilibria resulting from violent relaxation. In the cosmic density field predicted by a CDM model, the perturbations responsible for the formation of dark matter halos are expected to be clumpy, and so violent relaxation is expected to play some role in the formation of dark matter halos. However, as shown by N-body simulations, the density profiles of virialised dark matter halos *do* depend on the formation histories of dark halos (e.g. NFW; Klypin et al. 2001; Bullock et al. 2001; Eke et al. 2001; Wechsler et al. 2002; Zhao et al. 2003a,b; Tasitsiomi et al. 2004; Diemand et al. 2005). NFW conjectured that the dependence of halo concentration parameter on halo mass could be explained by the assembly of more massive halos at later times than lower-mass halos. Later, Wechsler et al. (2002) and Zhao et al. (2003a;b) found that the concentration of a halo depends on the assembly history. Together, these results suggest that CDM initial conditions play an important role in determining halo density profiles.

In this paper, we explore the relation between the density profile and the assembly histories of dark halos in CDM models. Our goal is to understand the physical processes that shape the density profiles of CDM halos, further motivated by the recent finding that the mass accretion histories of CDM halos show remarkable regularity. Based on high-resolution N-body simulations, the mass accretion history of a halo in general consists of two distinct phases: an early fast phase and a later slow phase (Wechsler et al. 2002; Zhao et al. 2003a,b; Li et al. 2005). As shown in Zhao et al. (2003a), the fast accretion phase is dominated by major mergers characterised by a rapid deepening of the halo potential. The slow accretion phase is characterised by only weak changes in the gravitational potential well. We will demonstrate that the 'universal' NFW profile results from gross properties of the mass accretion histories of dark matter halos. Using a simple spherical collapse model, we show that the inner profile is established in the fast accretion phase. Its key features are rapid collapse (in a small fraction of a Hubble time) with rapid changes in the potential that may isotropise the velocity field. The outer profile is dominated by particles that are accreted in the slow-accretion phase onto an existing central object. Our model incorporates these two phases of CDM accretion history to explain the appearance of 'universal' density profile in N-body simulations. In the absence of slow accretion, the outer profile would approach $\rho \propto r^{-4}$.

Our findings suggest that mass accretion history plays a crucial role in structuring halos.

The outline of this paper is as follows. In §2, we briefly describe CDM halo mass accretion histories, our procedure for realizing initial conditions for the formation of dark matter halos, and present our one-dimensional algorithm for simulating the collapse of dark matter halos. Our simulation results are described in §3. In §4, we use models with simple power-law initial perturbations to understand how NFW-like profiles are produced in CDM models. Finally, in §5, we further discuss and summarise our results.

2 INITIAL CONDITIONS AND METHODS

For a given halo, the mass accretion history specifies how much mass is added to the halo as a function of time. Numerical simulations and analytical models of halo formation in CDM models reveal that the mass accretion histories of CDM halos are remarkably regular. Wechsler et al. (2002) found that the accretion history of a CDM halos from N-body simulations can be described roughly by the following parametric form:

$$M(a) = M_0 \exp\left[-a_c S\left(\frac{a_0}{a} - 1\right)\right] , \qquad (2)$$

where a is the expansion scale factor of the universe, and M_0 is the virial mass of the halo at a final time where $a = a_0$. The formation history is characterised by a single parameter a_c. This characteristic scale factor $a = a_c$ is the point when the logarithmic mass accretion rate, $d\log M/d\log a$, falls below a critical value $S = 2$ (Wechsler et al. 2002). Similar results were found by Zhao et al. (2003a; b) using high-resolution simulations and by van den Bosch (2002) using extended Press-Schechter theory.

In a cosmological spherical collapse model, the shell collapse time is determined by the mean initial over-density within the mass shell; the mass within a mass shell collapses when the average linear over-density (calculated using linear perturbation theory) reaches $\delta_c \approx 1.686$. Therefore, for a given mass accretion history, we can then construct the corresponding initial density perturbation profile that reproduces this history. For a spherical perturbation of mass M that collapses at a redshift z, its linear over-density at the initial time z_i is given by

$$\delta_i(M) = 1.686 \frac{D(z_i)}{D(z)} , \qquad (3)$$

where $D(z)$ is the linear growth factor. In our calculation, we use the fitting formula by Carroll et al. (1992),

$$
\begin{aligned}
D(z) &= \frac{g(z)}{1+z} \qquad (4)\\
g(z) &\approx \frac{5}{2}\Omega_M(z)\left\{\Omega_M^{4/7}(z) - \Omega_\Lambda(z)\right.\\
&\left. + \left[1 + \frac{\Omega_M(z)}{2}\right]\left[1 + \frac{\Omega_\Lambda(z)}{70}\right]\right\}^{-1} , \qquad (5)
\end{aligned}
$$

where $\Omega_M(z)$ and $\Omega_\Lambda(z)$ are the density parameters of non-relativistic matter and of the cosmological constant at redshift z, respectively. At redshift z_i, the radius r_i of the sphere that encloses mass M is

$$r_i(M) = \left[\frac{3M}{4\pi \bar{\rho}(z_i)[1 + \delta_i(M)]} \right]^{1/3}, \qquad (6)$$

where $\bar{\rho}_i(z_i) = \rho_{\text{crit},0}\Omega_M(0)(1 + z_i)^3$, with $\rho_{\text{crit},0}$ the critical density of the universe at $z = 0$. Assuming that z_i is sufficiently large that the initial collapse is linear, equation (3) relates the enclosed mass $M(z)$ to its overdensity. Equation (6) then determines its radius at z_i. Choosing a mass partition $M_1 < M_2 < \cdots < M_N$, one can then determine the radii $r_1 < r_2 < \cdots < r_N$. We choose equal mass shells $m \equiv M_{j+1} - M_j$ for our simulations. Note that this procedure described by equations (3) and (6) is independent of the mass scale M_0 in equation (2) and, therefore, a single simulation may be scaled to any value of M_0 ex post facto.

We use one-dimensional particle simulations to explore the dynamical evolution of the collapse for a given mass accretion history. Note that even though the simulations are one-dimensional we can include the effects of angular momentum (see eq. 9 below). With a correction for the cosmological constant, we approximate the gravitational acceleration of the kth mass shell (particle) by

$$g_k = H_0^2 \Omega_\Lambda r_k - \frac{GM_k r_k}{(r_k^2 + \alpha^2)^{3/2}} \qquad (7)$$

$$M_k = \sum_{r_j < r_k} m_j \qquad (8)$$

where H_0 is Hubble's constant at the present time, Ω_Λ is the density parameter of the cosmological constant, r_k is the radius of the shell, and α is a softening length. In every simulation, we use a softening length $\alpha = 0.0005r_v$, where r_v is the virial radius of the halo at the present time. This scale is much smaller than any scale of interest. We assign each shell a specific angular momentum J_k; $J_k \equiv 0$ defines pure radial infall. The effective acceleration including the centrifugal force is then

$$a_k = g_k + \frac{J_k^2}{r_k^3} \qquad (9)$$

Since in spherical symmetry the gravitational force on a mass shell is determined by the mass enclosed by the mass shell, we calculate the force by sorting particles according to their radii. Owing to the finite number of shells, when two shells cross they experience a gravitational force discontinuity since then the enclosed mass instantly changes. To reduce such effects, we introduce another type of force softening. Instead of assuming that each shell is infinitesimally thin, we assume that it has a constant density with finite thickness, which we choose to be the distance between the interior and exterior neighbouring shells. Using such a softening method, crossing shells gradually change their enclosed mass and hence the gravitational forces change smoothly.

We use a time-symmetric symplectic leapfrog integrator (Quinn et al. 1997; Springel 2005) to solve the equations of motion. At each time step, we calculate the dynamical time for every shell and we choose the next time step to be smaller than the shortest dynamical time of all the shells, i.e.

$$\Delta t_{dyn} = \min_k \left\{ c_d \sqrt{\frac{5r_k^3}{2GM_k}} \right\}, \qquad (10)$$

where c_d is control parameter, which we set to be 0.001. Each simulation starts from an initial condition, which specifies
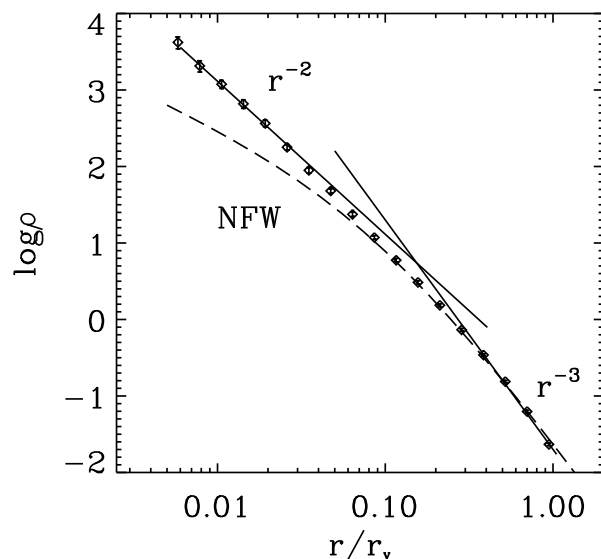
Figure 1. The diamonds are the binned density profile of a simulated dark matter halo at $z = 0$ with Poisson error bars. Particles are assumed to have pure radial motion in this simulation. Note that the outer density profile has $\rho \propto r^{-3}$, while the inner profile has $\rho \propto r^{-2}$. The dashed curve shows a NFW profile for comparison.

the position and velocity of each particle at a chosen high redshift. The position for each particle at the initial redshift z_i follows from the mass accretion history as described above. The initial velocity consists of two components: the Hubble expansion $v_i(M) = r_i(M)H(z_i)$ and the peculiar velocity. We use linear perturbation theory to relate the initial peculiar velocity of a mass shell to $\delta_i(M)$. We start our simulations at $z_i = 200$, early enough for linear theory to be valid.

All our simulations assume $\Omega_M = 0.3$ and $\Omega_\Lambda = 0.7$. We use 10^5 equal mass particles to simulate the formation of a single dark matter halo, and we have tested that this number is sufficiently large to achieve numerical convergence over the scales in which we are interested. In each simulation the total mass of all the particles is 1.2 times the final virial mass of the halo at $z = 0$. The extra mass maintains an ambient environment to follow the late stages of halo formation. As a test of our code we have reproduced the self-similar results of both Fillmore & Goldreich (1984) and Nusser (2001). We varied the particle number by a factor of 10, both larger and smaller, and could still satisfactorily reproduce these results.

3   RESULTS

We first consider a model with $a_c = 0.4$ corresponding to a formation redshift of $z_c = 1.5$ with pure radial motion ($J_k \equiv 0$ in eq. 9). The density profile of the halo at $z = 0$ is shown in Figure 1. The final $z = 0$ density profile has an inner logarithmic slope of -2 and an outer slope of -3. The predicted inner profile is much steeper than a NFW profile, although the model matches a NFW profile in the outer parts. We find that purely radial collapse simulations with

varying values of a_c all produce halo profiles with an inner logarithmic slopes of -2 and outer slopes of -3. Differing values of a_c affect only the transition radius between these two slopes; larger values of a_c (later formation times) leads to a larger transition radius, i.e. a lower concentration. Radial infall model alone cannot reproduce a NFW profile in the inner parts because it does not accurately represent the dynamics of fast accretion. The early fast accretion phase of a halo is dominated by major mergers and the depth of the potential well associated with the main progenitor deepens rapidly with time (Zhao et al. 2003a). Frequent scattering by potential fluctuations in this phase is expected to effectively isotropise the orbits. As a result, dark matter particles will acquire a significant amount of angular motion as they are accreted by the halo, which is not included in the purely radial calculation. However, the radial infall model does appear to successfully describe accretion from large distances onto an existing central mass in the slow accretion regime of halo formation and we will see in §4 that this does explain the agreement of the model with a NFW density profile in the outer parts. To simulate the fast accretion process more accurately using our one-dimensional approach, we consider a model that includes the effect of isotropic velocity dispersions. We trace the motion of each particle assuming pure radial motion into a radius of R_t, and at this point, we randomly assign a tangential component of velocity to the particle, keeping the kinetic energy unchanged. As the simulation evolves further, the angular momentum of each particle is conserved after an 'isotropisation' event. We choose R_t to be one half of the turn-around radius of each particle. Although this prescription seems somewhat arbitrary, a different choice only moderately shifts the radial scale. In detail, we incorporate this into our isotropisation prescription as follows. For a given mass shell M, we assume the ratio between the radial velocity dispersion, σ_r, and the tangential velocity dispersion σ_t, has the form,

$$\frac{\sigma_t^2}{\sigma_r^2} = 2\left[1 + \left(\frac{R_t}{r_a}\right)^\beta\right]^{-1}, \tag{11}$$

where r_a is the characteristic scale of the halo demarcating fast and slow accretion and β controls the shape of the anisotropy profile. The radial and tangential velocities are randomly sampled from Gaussian distributions. The ratio of these two random numbers are then used to partition the kinetic energy of the particle into radial and tangential components. For mass shells with $R_t \ll r_a$, the velocity distribution is nearly isotropic, while for those with $R_t \gg r_a$ radial orbits dominate. Note that a larger β produces a sharper transition between radial and isotropic orbits. We take $\beta = 2$ as our fiducial model and will describe the effect of changing the value of β below.

Since R_t is roughly the virial radius of a mass shell, we take $r_a = r_v(a_c)$, where $r_v(a_c)$ is the virial radius of the halo at the transition time between the fast accretion phase and the slow accretion phase. Figure 2 shows the final halo density profile of such a simulation. The resulting inner density profile is much flatter than the $\rho \propto r^{-2}$ we find for pure radial motions, and now over a large range of radius it can be well fit by a NFW profile. The inner profile is dominated by particles accreted in the fast accretion regime, and the shallower profile owes to the non-radial motions of these particles. These results are not particular to the mass accretion
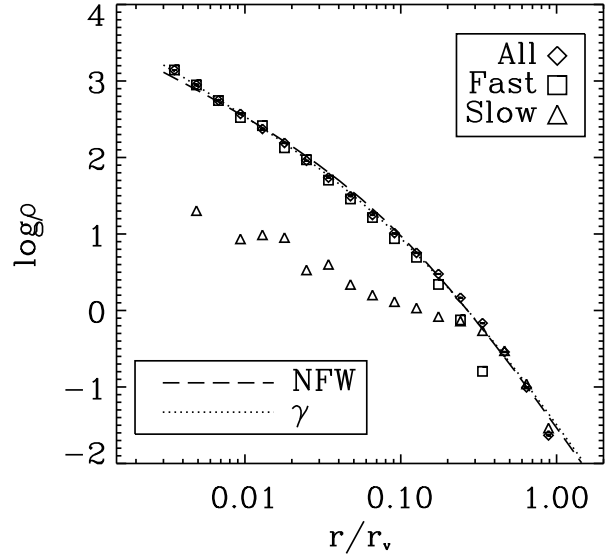

Figure 2. The density profile of a dark matter halo (diamonds) in a simulation where particles accreted in the fast accretion phase are assumed to have isotropic velocity dispersion (see text for details). The simulated density profile can be fit by a NFW profile (dashed curve). The dotted curve is the result of the best fit to the data by equation (12), and the best-fit value for γ is 1.21. Squares show the density profile for particles that are accreted in the fast accretion phase, while triangles show the density profile for particles accreted in the slow accretion phase. Note that the outer part of the halo profile is dominated by particles in slow accretion, while the inner profile is dominated by particles in the fast accretion phase.

history used in this example, and indeed our simulations with other mass accretion histories (see below) all lead to similar results.

We check the sensitivity to our velocity structure assumptions by varying the values of the two parameters r_a and β in equation (11). We first consider two alternatives to the fiducial model $r_a = r_v(a_c)$: $r_a = 0.5r_v(a_c)$ and $2r_v(a_c)$ with fixed $\beta = 2$. The density profiles given by these two models are shown in the left panel of Figure 3. The density profile changes very little even though the value of r_a changes by a factor of 4. Next, we hold r_a fixed at our fiducial value of $r_v(a_c)$ and vary the value of β from 0.5 to 10. The resulting density profiles are shown in the right panel of Figure 3. The final profile is also insensitive to changes in β.

In summary, if particles accreted in the fast accretion regime are assumed to have an isotropic velocity dispersion, we find that the inner slope of the halo density profile always lies in the range between -1 and -1.2. Apparently, the inner $\rho \propto r^{-1}$ profile is a generic result of the fast collapse phase and the isotropic velocity field generated during such a collapse.

The results obtained above can be compared to those obtained earlier by Avila-Reese et al. (1998) and Ascasibar et al. (2004). These authors examined the density profiles of dark matter halos produced by spherical collapse in a CDM density field, assuming that the orbits retain a constant el-
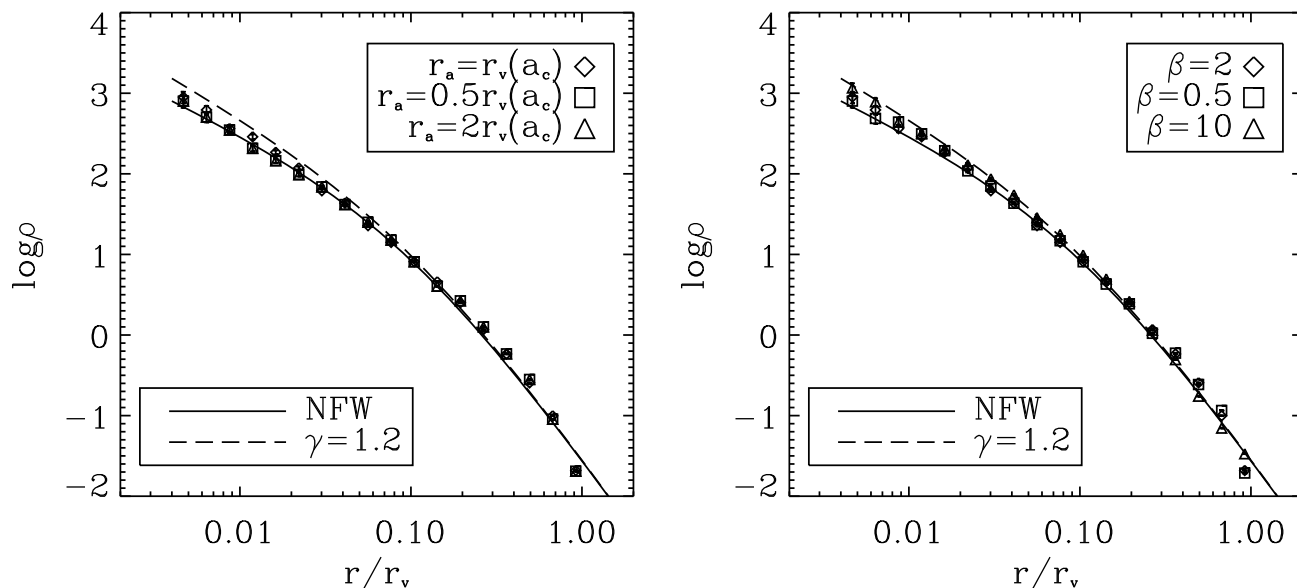
Figure 3. The density profiles for models with different choices of r_a and β [see equation (11) for definition]. In the left panel, results are shown for models where β is fixed to be 2 but r_a changes from $r_v(a_c)$ (diamonds) to $0.5r_v(a_c)$ (squares) and $2r_v(a_c)$ (triangles). In the right panel, r_a is fixed to be $r_v(a_c)$ but the value of β changes from 2 (diamonds) to 0.5 (squares) and 10 (triangles). The solid curve shows a NFW profile, while the dashed curve shows the profile (eqn. 12) with $\gamma = 1.2$.

lipticity. These models can produce NFW-like profiles provided that the constant ellipticity is properly chosen. However, as we describe in §4, spherical collapse with constant ellipticity orbits can produce a wide range of inner profiles depending on initial conditions. A good match between their models and the NFW profile requires a fine tuning of initial conditions. Shapiro et al. (2004) also explored the importance of CDM accretion history using one-dimensional simulations and very similar arguments to ours. Unfortunately, they use a fluid approach that solves Jeans-like moments of the collisionless Boltzmann equation and, presumably, the elimination of any possible asymmetric velocity distribution prevented them from finding our $\rho \propto r^{-1}$ result.

In contrast to these models, our consideration is based on realistic CDM halo formation histories. We demonstrate that, for all such formation histories, the early fast accretion of dark matter that may effectively generate an isotropic velocity dispersion leads naturally to $\rho \propto r^{-1}$ in the inner parts. Our isotropisation assumption is supported by the measurement of halo velocity dispersions in cosmological N-body simulations, which becomes progressively more isotropic towards the inner part of dark halos (e.g. Eke et al. 1998; Colín et al. 2000; Fukushige & Makino 2001; Hansen & Moore 2004).

We can study the dependence of halo structure on the 'formation time', characterised by a_c, using our one-dimensional simulations. We fit the resulting density profiles both with a NFW profile and one with the following more general form:
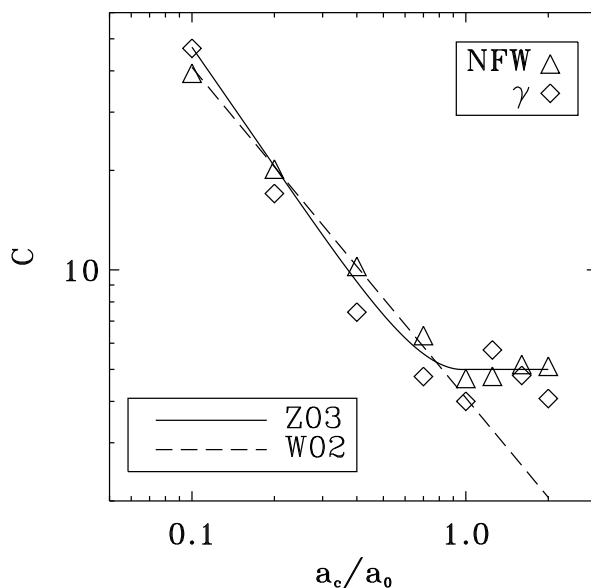

Figure 4. Halo concentration as a function of a_c, which characterises the halo formation time. Triangles show the results where simulated halo profiles are fit with a NFW profile and the diamonds are the results when fit with equation (12). The solid curve shows the prediction of a model proposed by Zhao et al. (2003a) based on cosmological N-body simulations, while the dashed curve shows the model prediction given by Wechsler et al. (2002).

$$\rho(r) = \frac{\rho_s}{(r/r_s)^\gamma \, [1 + (r/r_s)]^{(3-\gamma)}} \,, \qquad (12)$$

where γ is the inner slope of the profile. Figure 4 shows the best fit value of the concentration parameter, defined as $c \equiv r_v/r_s$, as a function of a_c. As one can see, halos with lower a_c, i.e. earlier formation times, are more concentrated. However, for halos that are still in the fast accretion phase, i.e. with $a_c > 1$, the concentration is independent of a_c. The solid curve shows the concentration-formation time relation obtained by Zhao et al. (2003a;b) using high-resolution N-body simulations. Our results assuming a NFW profile match this relation extremely well. The dashed line shows the model proposed by Wechsler et al. (2002). This model agrees well with our results for $a_c < 1$, but underestimates the concentration for halos with $a_c > 1$. We refer readers to Zhao et al. (2003a;b) for a detailed discussion about the discrepancy between their results and those obtained by Wechsler et al. (2002). Since it is known that the concentration-formation time relation is the origin of the mass-concentration relation (Wechsler et al. 2002, Zhao et al. 2003a), our results will also reproduce the mass-concentration relation (at a given redshift) as well as the concentration-redshift relation (at fixed mass) found in the cosmological N-body simulations.

So far, our discussion is based on simulations that assume the smooth accretion history given by equation (2). Although this smoothed form is a good description of the accretion history averaged over an ensemble of simulated dark halos, an individual accretion history exhibits details that are not described by equation (2). In some cases, equation (2) even fails to describe the overall shape of the mass accretion history. We show such an example in the left panel of Figure 5. A fit that emphasises the accretion history before the big jump at $a = 0.45$, shown by the short dashed curve, differs from a fit that emphasises the history after that time. To see how such differences affect the density profiles, we carried out one-dimensional simulations using realistic halo accretion histories generated by PINOCCHIO, a Lagrangian code developed by Monaco et al. (2002). The statistical properties of the mass accretion histories generated using this code agrees with those obtained using cosmological N-body simulations (Li et al. 2005). The resulting simulated halo density profiles can all be well described by the NFW form. For many cases where equation (2) is a good fit to the overall accretion history, the simulated density profiles using real accretion histories are very similar to those using the corresponding fits with equation (2). Even for cases where the accretion history is poorly described by equation (2), as the one shown in Figure 5a, the final halo profile can still be well fit using a NFW form (see Fig. 5b). In such cases, however, the formation time defined using equation (2) is uncertain.

The difference in the detailed mass accretion history introduces a scatter in the distribution of the concentration parameter c (Wechsler et al. 2002). If the density profile is determined by its mass accretion history, then we should be able to reproduce the distribution of c using a random sample of realistic mass accretion histories. To perform this experiment, we have randomly chosen 50 mass accretion histories generated with PINOCCHIO for halos with masses in the range $10^{11} - 10^{12}$ M$_\odot$. These mass accretion histories are used to generate initial conditions for our one-dimensional simulations. Figure 6 shows the distribution of the concentration parameter, obtained by fitting the simulated profiles
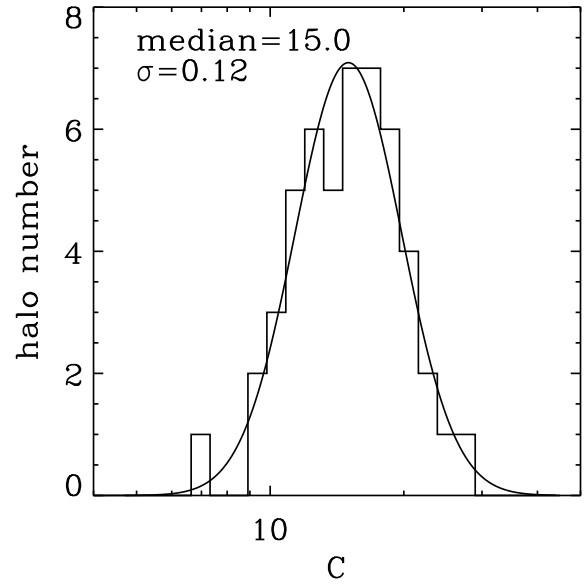

Figure 6. The histogram shows the distribution of halo concentration obtained from an ensemble of 50 randomly chosen mass accretion histories for halos with masses in the range 10^{11} M$_\odot$ to 10^{12} M$_\odot$ at the present time. The solid curve shows a log-normal distribution with a median equal to 15.0 and a dispersion (in $\log c$) equal to 0.12.

with the NFW form. The distribution can be roughly described by a log-normal, in agreement with the cosmological N-body results (e.g. Jing 2000; Bullock et al. 2001). The dispersion in $\log c$, $\sigma = 0.12$, is also very close to that found in cosmological N-body simulations (e.g. Wechsler et al. 2002), reinforcing our finding that the density profile of a halo is largely determined by its mass accretion history.

4 WHAT DETERMINES THE DENSITY PROFILES OF DARK MATTER HALOS?

In the last section, we have shown that many of the structural properties of CDM halos found in cosmological N-body simulations can be understood in terms of halo mass accretion histories. However, why does gravitational collapse with such initial conditions always produce halo profiles that follow a universal form? Is the universal profile a result of the fact that the initial conditions represented by CDM mass accretion histories are special, or is it more generic in the sense that it can be produced by a wide range of initial conditions?

To answer this question, we consider the collapse of generic initial perturbations with the form

$$\frac{\delta M(r)}{M(r)} \propto M(r)^{-\epsilon}, \tag{13}$$

where ϵ is a constant that controls the mass accretion rate. Because a mass shell collapses when $\delta M/M \approx 1.68$, the mass accretion history implied by equation (13) is $M(z) \propto D^{1/\epsilon}(z)$, where $D(z)$ is the linear growth factor. Since the circular velocity of a halo V_c is related to its mass, $M \sim V_c^3/H(z)$, where $H(z)$ is the Hubble constant at redshift z,
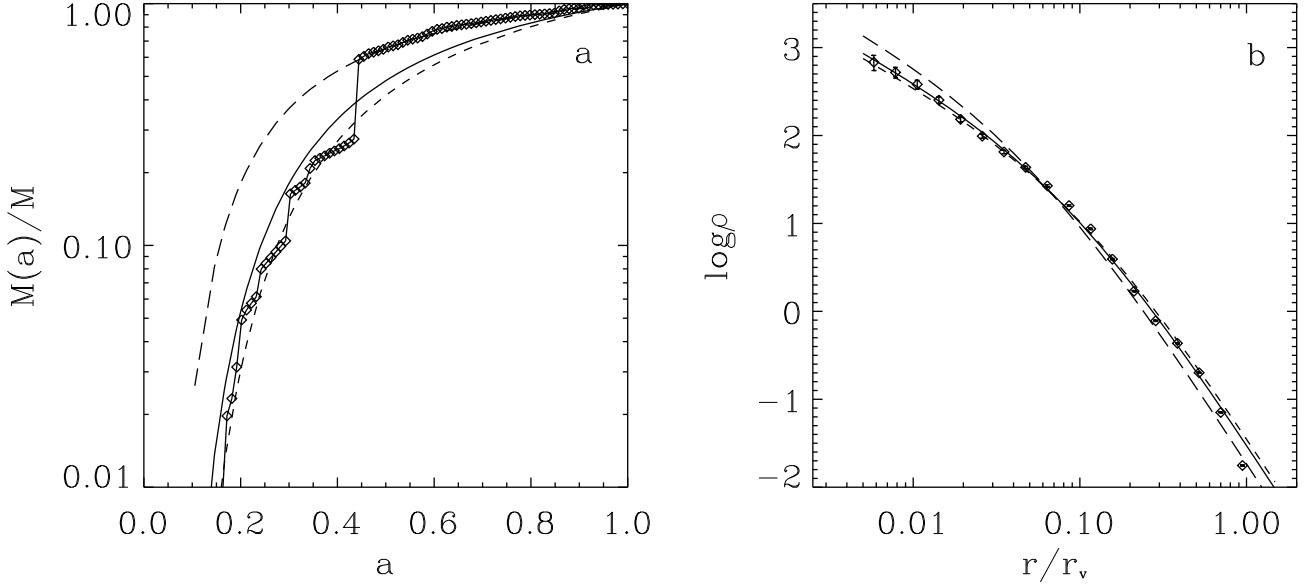
Figure 5. The diamonds in panel (a) show a mass accretion history that cannot be well fit using equation (2). The long (short) dashed curve is the result of fit that emphasises the recent (past) history at $a > 0.45$ ($a < 0.45$). The solid curve represents a compromise between the recent and past histories. The halo profiles corresponding to the actual mass accretion history and these three possible fits are shown in panel (b).

we can write $V_c(z) \propto H^{1/3}(z)D^{1/3\epsilon}(z)$. For simplicity, we consider an Einstein-de Sitter universe. In this case, $D \propto H^{-2/3}$, and therefore

$$M \propto H^{-2/3\epsilon}, \qquad V_c \propto H^{(1-2/3\epsilon)/3}. \qquad (14)$$

Note that V_c^2 is a measure of the depth of potential well associated with the halo. For $\epsilon = 1/6$, $V_c \propto H^{-1}$ ($M \propto H^{-4}$). Therefore, $\epsilon = 1/6$ separates the isotropisation regime from calm accretion, i.e. V_c changes by an order of unity or more in a Hubble time for $\epsilon < 1/6$. For $\epsilon = 2/3$, $M \propto H^{-1}$ ($V_c = $ constant) and, similarly, $\epsilon = 2/3$ separates fast accretion from slow accretion in terms of the mass accretion rate. For $\epsilon \to 0$, perturbations on different mass scales have the same amplitude, and all mass scales collapse simultaneously, leading to fast increases in both mass and potential well depth. In contrast, for $\epsilon \gg 1$ the perturbation amplitude declines rapidly with mass scale, hence M increases little while the potential well decays as the universe expands. This allows us to study cases with vastly different collapse histories by changing the value of ϵ over a large range.

In an Einstein-de Sitter universe where the expansion factor a is a power law of time, the collapse of perturbations described by equation (13) admits similarity solutions. Assuming spherical symmetry and pure radial motion, Fillmore & Goldreich (1984) show that the collapse develops an asymptotic density profile $\rho \propto r^{-\gamma}$ in the inner region, with $\gamma = 2$ for $0 < \epsilon \leq 2/3$, and $\gamma = 9\epsilon/(1+3\epsilon)$ for $\epsilon > 2/3$. These solutions are shown in Figure 7 as the long-dashed curve. Self-similar models can also be constructed for non-radial motions (Nusser 2001). The specific angular momentum of a particle can be specified as

$$J = \mathcal{J}\sqrt{GM_{ta}r_{ta}}, \qquad (15)$$

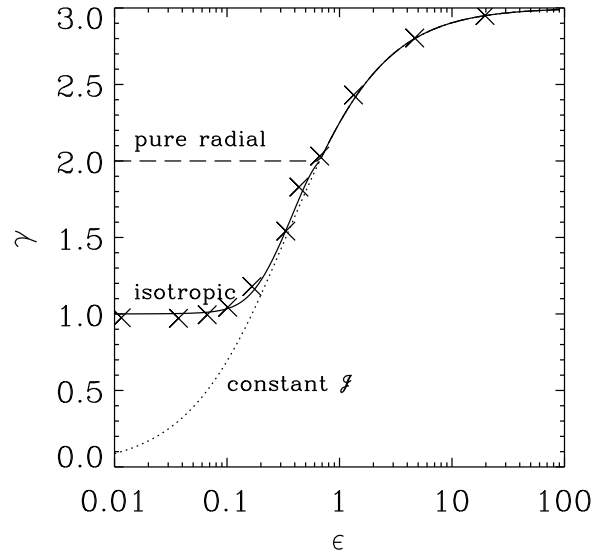**Figure 7.** The relation between the inner logarithmic slope, γ ($\rho \propto r^{-\gamma}$), as a function of the exponent of the initial perturbation defined in equation (13). The long dashed curve shows the solution of the model with pure radial motion and the dotted curve shows the solution when all particles have the same $\mathcal{J}$. The solution with an isotropic velocity dispersion is shown as the solid curve, and is compared with the result obtained directly from numerical calculations (crosses). All the three curves overlap for $\epsilon \geq 2/3$.

where $r_{\rm ta}$ is the turnaround radius of the particle, and $M_{\rm ta}$ is the mass interior to $r_{\rm ta}$. If $\mathcal{J}$ is the same constant for all particles, the problem admits similarity solutions and the asymptotic inner slope of the density profile is $\gamma = 9\epsilon/(1 + 3\epsilon)$ for all $\epsilon > 0$ (Nusser 2001). This solution is shown as the dotted curve in Figure 7. For $\epsilon \geq 2/3$, this solution is the same as that for the model with pure radial infall. The asymptotic value of γ is 0 as $\epsilon \to 0$. The dependence of γ on ϵ for a constant $\mathcal{J}$ is steep near $\gamma \sim 1$. Thus, to produce a NFW inner slope in this model requires tuned initial conditions.

For our models in §3, the velocity dispersion of particles in the early collapse phase is isotropic. Thus, the quantity $\mathcal{J}$ has the following distribution at fixed energy:

$$P(\mathcal{J}) = \frac{\mathcal{J}}{\sqrt{1 - \mathcal{J}^2}} \,. \tag{16}$$

For the slow accretion phase, we expect the results of pure radial motion to obtain. Thus, for $\epsilon \geq 2/3$, the asymptotic slope is $\gamma = 9\epsilon/(1 + 3\epsilon)$. For $\epsilon < 2/3$, we can also use a simple model to understand the results obtained in the last section. Consider all particles with a given $\mathcal{J}$. In general, we can write the final density profile of these particles as $\Delta\rho_{\mathcal{J}}(r) \propto (\Delta M_{\mathcal{J}}/r_{\mathcal{J}}^3)F(r/r_{\mathcal{J}})$, where $\Delta M_{\mathcal{J}}$ is the total mass of particles with $\mathcal{J}$ in the range $\mathcal{J} \pm \Delta\mathcal{J}$, and $r_{\mathcal{J}}$ is a characteristic scale in the density profile. The quantity $\Delta M_J/r_J^3$ is the density scale. Since the only scale in the problem is the current turnaround radius $r_{\rm out}$, and since non-radial motion is expected to be important only for $r \ll \mathcal{J}r_{\rm out}$, we expect $r_{\mathcal{J}} \propto \mathcal{J}r_{\rm out}$. Thus,

$$\Delta\rho_{\mathcal{J}}(r) \propto \frac{M}{r_{\rm out}^3} \frac{P(\mathcal{J})\Delta\mathcal{J}}{\mathcal{J}^3} F\left(\frac{r}{\mathcal{J}r_{\rm out}}\right) \,. \tag{17}$$

If we neglect the interaction between mass shells of different $\mathcal{J}$, the total density can be written as

$$\rho(r) = \sum \Delta\rho_{\mathcal{J}}(r) \propto \frac{M}{r_{\rm out}^3} \int_0^1 \frac{P(\mathcal{J})\mathrm{d}\mathcal{J}}{\mathcal{J}^3} F\left(\frac{r}{\mathcal{J}r_{\rm out}}\right) \,. \tag{18}$$

On scales where the effect of angular momentum is important, i.e. $r \ll \mathcal{J}r_{\rm out}$, the density profile is expected to be $F(r) \propto r^{-9\epsilon/(1+3\epsilon)}$. Conversely, for $r \gg \mathcal{J}r_{\rm out}$ the particles are in nearly radial motion and one expects $F(r) \propto r^{-2}$ (for $\epsilon < 2/3$). Hence, we may approximate the form of F as $F(x) = 1/[x^2 + x^{9\epsilon/(1+3\epsilon)}]$. Inserting this and equation (16) into equation (18), we obtain

$$\rho(r) \propto \frac{M}{r_{\rm out}^3} \frac{r_{\rm out}}{r}Q(\epsilon, r_{\rm out}/r) \,, \tag{19}$$

where

$$Q\left(\epsilon, r_{\rm out}/r\right) = \int_0^{\pi/2} \frac{(r_{\rm out}/r)\mathrm{d}\theta}{1 + [(r_{\rm out}/r)\sin\theta]^\alpha} \,, \tag{20}$$

with

$$\alpha \equiv \frac{2 - 3\epsilon}{1 + 3\epsilon} \,. \tag{21}$$

The inner density profile is given by the r dependence of Q for $r/r_{\rm out} \to 0$. The solid curve in Figure 7 shows the resulting γ-ϵ relation. The characteristics of this relation can be understood as follows. For $\epsilon < 1/6$, then $\alpha > 1$. The integration in Q is dominated by small θ, and so we can replace $\sin\theta$ by θ. The function Q is independent of r and $\rho \propto r^{-1}$. For $1/6 < \epsilon < 2/3$, then $0 < \alpha < 1$ and the

integration is now dominated by $\sin\theta > r/r_{\rm out}$. The function $Q \propto r^{\alpha-1}$ and, therefore, $\gamma = 9\epsilon/(1 + 3\epsilon)$. This relation between γ and ϵ holds also for $\epsilon > 2/3$, as discussed above.

To check the accuracy of the above simple model, we use a numerical calculation to solve for the inner density profile as a function of ϵ. For any radius r, the total mass within it can be written in two parts,

$$m_T(r) = m_p(r) + m_t(r) \,. \tag{22}$$

Here m_p is the mass of all particles with apocenter smaller than r. We call these particles 'permanent' contributors because they always contribute to $m_T(r)$. The mass m_t in the above equation is the contribution of particles with apocenter r_a larger than r but with a smaller pericenter r_b. These are 'temporary' contributors because they only spend part of their orbital times within r. Let $P(r|r_k)$ be the fraction of time that a 'temporary' particle with turnaround radius r_k spends inside radius r. The total mass contributed by temporary particles can be written as

$$m_t(r) = \int_{r_b < r < r_a} P(r|r_k)\mathrm{d}m(r_k), \tag{23}$$

where the measure includes all orbits that pass through the surface at r. By definition,

$$P(r|r_k) = \int_r^{r_a} \frac{\mathrm{d}r'}{v_k(r')} \Big/ \int_{r_b}^{r_a} \frac{\mathrm{d}r'}{v_k(r')} \tag{24}$$

where $v_k(r')$ is the radial velocity of a particle with turnaround radius r_k at a radius r'. Note that $v_k(r)$ as a function of r depends on the current mass profile $m_T(r)$, and so the mass profile has to be solved by iteration. The radial velocity can be written as

$$v_k(r) = \sqrt{2}\left[E_k - \Phi(r) - J_k^2/(2r^2)\right]^{1/2} \tag{25}$$

where E_k and Φ are, respectively, the total energy and gravitational potential of the particle, and J_k is the specific angular momentum. The increase of mass within the apocenter of a particle can change the orbit of the particle. Thus, we must recompute such changes at each step of the iteration. Assuming that angular momentum is conserved, the apocenter r_a of a particle after a given iteration is related to the apocenter r_a' before by $m_T(r_a)r_a = m_T'(r_a')r_a'$, where m_T' and m_T are the mass profiles before and after the iteration step. The iteration starts from an initial condition where each particle is at its turnaround radius, and we denote the corresponding profile by $M_{\rm ta}(r_{\rm ta})$. Since the turnaround radius $r_{\rm ta}$ of a mass shell is related to its initial radius r_i by $r_{\rm ta} \propto r_i(\delta M/M)^{-1}$ in an Einstein-de Sitter universe and since $M \propto r_i^3$, one can show that

$$M_{\rm ta}(r_{\rm ta}) \propto r_{\rm ta}^n, \quad n = 3/(3\epsilon + 1)\,. \tag{26}$$

We have applied the above numerical calculation to models with pure radial infall and models where $\mathcal{J}$ is the same for all mass shells. The results match those given by the self-similarity solutions. The crosses in Figure 7 show the γ–ϵ results for this calculation using an isotropic velocity dispersion given by equation (16). The numerical results match the simple analytical model presented above remarkably well. We have also applied our one-dimensional code to this model and the results are similar to those obtained here.

One important feature in the γ-ϵ relation predicted by this model is that $\gamma \approx 1$ for all $0 < \epsilon \lesssim 1/6$. For a perturbation with ϵ in this range, the circular velocity of the halo increases rapidly with time, with a timescale that is shorter than a Hubble time. In this case, not only can particles with small apocenters (low orbital energies) reach the inner part of the halo, but also can many particles with large apocenters (high orbital energies) and small angular momenta. Velocity isotropisation mixes these orbits, resulting in $\gamma \approx 1$ as we have demonstrated. For $\epsilon > 1/6$ the gravitational potential is changing gradually and particles joining the halo have a similar energy and orbital shape $\mathcal{J}$. The resulting profile can then be described by the self-similar solution that assumes the same orbital shape for all particles and γ becomes larger than one. Note that an inner logarithmic slope of approximately -1 results from a fast collapse and orbit isotropisation and that both conditions are required to produce such an inner slope. If the collapse is fast ($\epsilon \lesssim 1/6$) but the velocity dispersion is not isotropic, the inner slope can be as shallow as 0 (for constant $\mathcal{J}$) and as steep as -2 (for radial infall). If the velocity dispersion is isotropic, but the mass accretion rate is small, i.e. $\epsilon > 1$, the inner slope can be much steeper than -1.

The identification of this mechanism not only explains the approximate universality of the inner CDM halo slopes but also describes the variance observed in N-body simulations. Gravitational collapse starts on small scales in a hierarchical model such as CDM. Deep dark-matter potential wells are created by subsequent non-linear gravitational collapse, but the potential well associated with a halo cannot deepen significantly during the slow accretion phase when the accretion time scale is longer than a Hubble time (Zhao et al. 2003a). Therefore, all halos must have gone through a phase of rapid accretion to establish their potential wells, even though different halos may have different mass accretion histories. Also, as shown in Li et al. (2005), the phase of rapid mass accretion is dominated by major mergers, which may effectively isotropise the velocity field. These are the two ingredients that are required to produce a $\rho \propto r^{-1}$ inner profile, and explain why such a inner profile results for halos with vastly different formation histories. If the potential well of a halo is established at early times, the mass contained in the r^{-1} profile will be small, and the halo will have a high concentration since most of the mass accreted slowly. However, if a halo establishes its potential well recently, much of its mass will be in the r^{-1} profile, and the halo will have a low concentration. This correlation between halo concentration and the time of potential well formation matches cosmological N-body simulations (e.g. Zhao et al. 2003a;b). In extreme cases where the mass involved in the fast accretion is too small to be seen, we expect an inner profile steeper than r^{-1}.

So far we have only considered the origin of the inner r^{-1} profile. What about the outer r^{-3} form in the universal profile? Consider a shell of mass M and of an initial radius r_i. Suppose this mass shell collapses at a time t to a radius r. Assuming an Einstein-de Sitter Universe and neglecting the effect of shell crossing, we have $r \propto r_i/\delta_i(M)$ and $t \propto t_i/\delta_i(M)^{3/2}$. Eliminating $\delta_i(M)$ in these two relations and using $M \propto r_i^3$ we obtain $r \propto M^{1/3}t^{2/3}$. Thus, the density profile can be written as

$$\rho(r) = \frac{1}{4\pi r^2}\frac{\mathrm{d}M}{\mathrm{d}t}\left(\frac{\mathrm{d}r}{\mathrm{d}t}\right)^{-1} \propto \frac{M}{r^3}\frac{\mu}{2+\mu}, \qquad (27)$$

where $\mu \equiv \mathrm{d}\ln M/\mathrm{d}\ln t$. Now let us write the mass in two parts, $M = M_e + \Delta M$, where M_e is the mass of the halo at $t - \Delta t$, while ΔM is the mass accreted between time $t - \Delta t$ and t. If ΔM increases as a power law of t, and if $\Delta M \ll M_e$, then $\rho \propto r^{-3}$. Since a mass shell settles into an equilibrium state over several dynamical times, the relevant scale for Δt is the dynamical time of the system. Thus, if there is a period of slow accretion, but where the total accreted mass is much smaller than the mass that has collapsed into the halo, an outer density profile with $\sim r^{-3}$ results. However, the above argument also suggests that the outer density profile can change from halo to halo, depending on the mass accretion rate at the final stage of halo formation. For example, if M continues to grow as described by equation (2) eventually a density profile with $\rho \propto r^{-4}$ in the outer parts will result.

To demonstrate such a dependence of the outer profile on mass accretion history, we have carried out 1-D simulations for three cases with different recent mass accretion histories. These mass accretion histories are shown in the left panel of Figure 8, and the resulting logarithmic slopes versus r are shown in the right panel. This figure shows that while halos with typical mass accretion histories have $\rho \propto r^{-3}$ outer density profiles, halos with slower accretion rates in the recent past (shown by the dashed and dotted curves) have steeper outer profiles. Therefore, the outer r^{-3} profile is not universal but a consequence of the form of mass accretion history of typical CDM halos and in the currently accepted cosmological model all halos will have a r^{-4} outer profile in the distant future.

5 SUMMARY AND DISCUSSION

We have constructed a simple model that reproduces many of the properties of the CDM halo population. There are two essential ingredients: 1) a two-phase accretion history beginning with rapid accretion and potential-well deepening followed by slow accretion with little change in the potential well; and 2) isotropisation of orbits during the phase of rapid growth. The density profiles obtained from various mass accretion histories all fit the NFW form. Our model also reproduces the correlation between the concentration and formation time observed in cosmological N-body simulations. In particular, the model predicts a roughly constant concentration, $c \sim 5$, for all halos that are still in the fast accretion phase, matching the results obtained by Zhao et al. (2003a;b). Combined with an ensemble of realistic mass accretion histories parametrised from cosmological CDM simulations, the model reproduces the dependence of halo concentration on halo mass and the distribution of halo concentrations measured in these same cosmological N-body simulations. Our results demonstrate that the structural properties of CDM halos are largely determined by their mass accretion histories.

We can recover many of these results using a simple analytic model. Our model begins with scale-free perturbations of the form $\delta M(r)/M(r) \propto M(r)^{-\epsilon}$ in an Einstein-de Sitter universe. Assuming an isotropic velocity dispersion, we find that the inner profile produced by the collapse of such perturbations is always a power law, $\rho(r) \propto r^{-\gamma}$, with
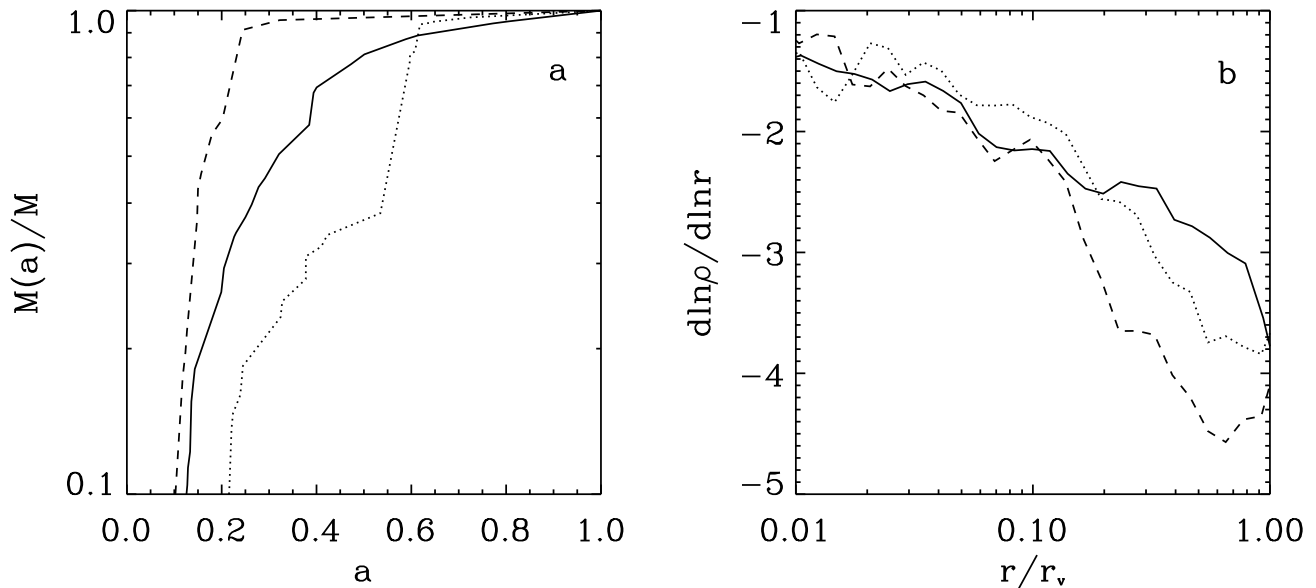
Figure 8. The left panel shows three mass accretion histories that have different accretion rates in the recent past. The right panel shows, as a function of radius, the logarithmic slope of the density profile generated with each of these three mass accretion histories. Note that the outer slope can be as steep as -4 for a halo whose recent mass accretion rate is very small (dotted and dashed curves).

$\gamma = 1$ for $0 < \epsilon < 1/6$, and $\gamma = 9\epsilon/(1 + 3\epsilon)$ for $\epsilon > 1/6$. A model with $0 < \epsilon < 1/6$ has a rapidly deepening potential leading to orbit isotropy. This produces a shallower profile than a purely radial model. Assuming non-radial orbits of constant shape yields self-similar models but with a large range of possible inner slopes. The mixture resulting from isotropisation converges to a single inner slope $\rho \propto r^{-1}$. This suggests that the inner r^{-1} profile of CDM halos is a natural result of hierarchical models, where the potential well associated with a halo has to be built through a phase of rapid and violent accretion in which potential fluctuations are expected to effectively isotropise the velocities of CDM particles.

As mentioned in the introduction, a number of authors have previously noticed that tangential motions of particles can cause flattening in the inner density profile of dark matter halos (e.g. White & Zartisky 1992; Ryden 1993; Sikivie et al. 1997; Subramanian et al. 2000; Subramanian 2000; Hiotelis 2002; Le Delliou & Henriksen 2003; Shapiro et al. 2004; Barnes et al. 2005). Applying the collisionless Boltzmann equation to self-similar gravitational collapse, Subramanian (2000) and Subramanian et al. (2000) demonstrated that tangential velocities are required to obtain an inner profile that is shallower than that of a singular isothermal sphere. They suggested that an appropriate mixture of radial and tangential velocities may produce an inner r^{-1} profile. However, these authors did not propose a specific model that predicts such a profile. Furthermore, as we have shown in this paper, isotropic velocity dispersion alone is not sufficient for generating an inner r^{-1} profile; rapid accretion with a quickly deepening potential well is also required in our model. Thus, although our explanantion about the inner density profile of dark matter halos is related to those pre-

sented in these earlier analyses, it provides additional physical insight into the problem, in particular in connection to the properties of the mass accretion history that influence the final density profile.

Since our model only relies on the mass accretion history and orbit isotropisation to explain the origin of NFW profiles, it naturally explains why collapses with artificially reduced substructure (Moore et al. 1999) also lead to the universal profile, even when the initial condition is as smooth as three intersecting plane waves (Shapiro et al. 2004). However, if it is so smooth that the orbits are not isotropised then a steeper central slope may result. Note that although our explanation depends on different mass accretion histories it does not explicitly depend on the dynamical friction and tidal distribution of the substructures that makes up the actual mass accretion in cosmological N-body simulations (e.g. Dekel et al. 2003).

It is remarkable that our one-dimensional simulations with their two simple ingredients reproduce the structural features of the full three-dimensional simulations. In retrospect, this result is consistent with the physical nature of hierarchical formation. Because dark-matter halos are extended, even equal mass mergers are relatively quiescent, their mutual orbits slowly decaying by dynamical friction and ending with a low velocity merger, tidal dissolution, and phase mixing. Such events are likely to produce sufficient scattering to yield isotropisation but not as violent as envisioned by Lynden-Bell (1967). Therefore, once we have the two necessary ingredients, the final equilibrium profile may not be sensitive to the exact way in which the system settles into its final equilibrium configuration. Zhao et al. (2003a) show that a significant correlation still exists between the final and initial binding energies even for particles that are

accreted in the fast accretion phase based on 5 halos in their high-resolution simulations. Reinforcing this point, we also find that the final energy of a particle is correlated with its initial energy, and hence the energy distribution of particles is determined by the initial conditions rather than by complete relaxation. The match between our one-dimensional model and the three-dimensional cosmological simulations suggests that violent relaxation might not play an important role in redistributing the energies of particles except through isotropising the velocity field.

ACKNOWLEDGMENTS

REFERENCES

Ascasibar Y., Yepes G., Gottlöber S., Müller V., 2004, MNRAS, 352, 1109
Avila-Reese V., Firmani C., Hernández X., 1998, ApJ, 505, 37
Barnes E.I., Williams L.L.R., Babul A., Dalcanton J.J., 2005, ApJ, 634, 775
Bertschinger E., 1985, ApJS, 58, 39
Bullock J.S., Kolatt T.S., Sigad Y., Somerville R.S., Kravtsov A.V., Klypin A.A., Primack J.R., Dekel A., 2001, MNRAS, 321, 559
Carroll S. M., Press W. H., Turner E. L. 1992, ARAA, 30, 499
Colín P., Klypin A.A., Kravtsov A.V., 2000, ApJ, 539, 561
Dekel A., Arad I, Devor J., Birnboim Y, 2003, ApJ, 588, 680
Diemand J., Zemp M., Moore B., Stadel J., Carollo M., 2005, MNRAS, 364, 665
Eke V.R., Navarro J.F., Frenk C.S., 1998, ApJ, 503, 569
Eke V.R., Navarro J.F., Steinmetz M., 2001, ApJ, 554, 114
Fillmore J.A., Goldreich P., 1984, ApJ, 281, 1
Fukushige T., Makino J., 1997, ApJ, 477, L9
Fukushige T., Makino J., 2001, ApJ, 557, 533
Fukushige T., Makino J., 2003, ApJ, 588, 674
Ghigna S., Moore B., Governato F., Lake G., Quinn T., Stadel J., 2000, ApJ, 544, 616
Gott J.R., 1975, ApJ, 201, 296
Gunn J.E., 1977, ApJ, 218, 592
Gunn J.E., Gott J.R., 1972, ApJ, 176, 1
Hansen S.H., Moore B., 2004, preprint, astro-ph/0411473
Hiotelis N., 2002, A&A, 382, 84
Hoffman Y., Shaham J., 1985, ApJ, 297, 16
Huss A., Jain B., Steinmetz M., 1999, ApJ, 517, 64
Jing Y.P., 2000, ApJ, 535, 30
Jing Y.P., Suto Y., 2000, ApJ, 529, L69
Klypin A., Kravtsov A.V., Bullock J.S., Primack J.R., 2001, ApJ, 554, 903
Le Delliou M., Henriksen R.N., 2003, A&A, 408, 27
Li Y., Mo H.J., vand den Bosch F.C., 2005, preprint, astro-ph/0510372
Lynden-Bell D., 1967, MNRAS, 136, 101
Monaco P., Theuns T., Taffoni G., 2002, MNRAS, 331, 587
Moore B., Quinn, T., Governato F., Stadel J., Lake G., 1999, MNRAS, 310, 1147
Navarro J.F., Frenk C.S., White S.D.M., 1996, ApJ, 462, 563
Navarro J.F., Frenk C.S., White S.D.M., 1997, ApJ, 490, 493
Nusser A., 2001, MNRAS, 325, 1397
Quinn T., Katz N., Stadel J., Lake G., 1997, preprint, astro-ph/9710043
Ricotti M., 2003, MNRAS, 344, 1237
Ryden B.S., 1988, ApJ, 333, 78
Ryden B.S., 1993, ApJ, 418, 4
Ryden B.S., Gunn J.E., 1987, ApJ, 318, 15
Shapiro P.R., Iliev I.T., Martel H., Ahn K., Avarez M.A., 2004, preprint, astro-ph/0409173
Sikvie P., Tkachev I.I., Wang Y., 1997, Phys. Rev. D, 56, 1863
Springel V., 2005, MNRAS, 364, 1105
Subramanian K., 2000, ApJ, 538, 517
Subramanian K., Cen R., Ostriker J.P., 2000, ApJ, 538, 528
Taylor J.E., Navarro J.F., 2001, ApJ, 563, 483
Tasitsiomi A., Kravtsov A.V., Gottloeber S., Klypin A.A., 2004, ApJ, 607, 125
Tremaine S., Henon M., Lynden-Bell D., 1986, MNRAS, 219, 285
van Albada T.S., 1982, MNRAS, 201, 939
van den Bosch F. C., 2002, MNRAS, 331, 98
Wechsler R.H., Bullock J.S., Primack J.R., Kravtsov A.V., Dekel A., 2002, ApJ, 568, 52
White S. D. M., Zaritsky D., 1992, ApJ, 394, 1
Zaroubi S., Hoffman Y., 1993, ApJ, 416, 410
Zhao D., Mo H.J., Jing Y.P., Börner G., 2003a, MNRAS, 339, 12
Zhao D., Jing Y.P., Mo H.J., Börner G., 2003b, ApJ, 597, L9